Transport Anisotropy and Impurity Scattering in Ge at Millikelvin Temperatures: Experimental Study

E. Olivieri, J. Domange, L. Dumoulin, S. Marnieros, A. Broniatowski

Transport Anisotropy and Impurity Scattering in Ge at Millikelvin Temperatures: Experimental Study

E. Olivieri[1], J. Domange[1,2], L. Dumoulin[1], S. Marnieros[1] and A. Broniatowski[1(*)]

[1]*Centre de Spectrométrie Nucléaire et de Spectrométrie de Masse, IN2P3/CNRS and Université Paris XI, Bât. 108, 91405 Orsay (France)*
[2]*CEA/IRFU/SPP, 91191 Gif-sur-Yvette (France)*

Anisotropy effects in hot carrier transport have been investigated in germanium crystals at mK temperatures in the electric field range pertaining to the operation of the Edelweiss dark matter detectors. Comparative measurements have been made on n-type specimens of different impurity contents, both ultra-pure (N_d-N_a < 10^{10} cm^{-3}) and doped to 10^{11} cm^{-3}. At relatively high field intensities (> ~ 5 V/cm), similar features of electron and hole transport are observed independent of the concentration of electrically active impurities. Differences appear at lower field (down to a fraction of a V/cm) with regard to electron straggling especially, dependent on crystal purity. These experiments demonstrate the importance on carrier transport of impurity scattering at low field, whereas phonon scattering becomes the dominant factor at higher field intensities.

1. INTRODUCTION

Anisotropy in hot carrier transport is a well-known property of germanium semiconducting crystals,[1,2] whose effects on charge collection in cryogenic Ge detectors for dark matter search remain however to be investigated in depth. Large effects of carrier straggle are expected in the case of the electrons especially, due to their effective mass anisotropy and the multivalleyed character of the conduction band[3,4]. (Straggling refers to the

(*) corresponding author. e-mail: alexandre.broniatowski@csnsm.in2p3.fr

effects on carrier motion, arising from their random scatter by phonons, impurities and crystal defects.) The purpose of this paper is to characterize these features of electron and hole transport, and the way they reflect in the detector response to a particle. An experimental setup is implemented, enabling to investigate electron and hole collection separately, and to quantify their respective straggles as a function of the detector bias. A comparison of the patterns of charge collection in crystals different by their impurity content demonstrates the importance, besides phonons, of impurity scattering in explaining these features of carrier transport, particularly in the low field conditions (a few V/cm) typical for the operation of these devices.
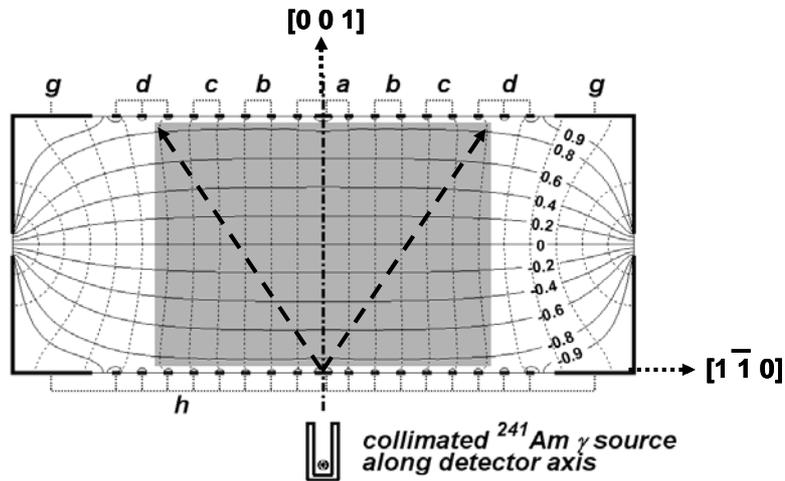
Fig. 1. Detector crystal in cross-section along the (1 1 0) plane, showing the connection scheme of the electrodes and the different charge measurement channels (see text). The equipotentials (full lines) and the field lines (dotted lines) are drawn for detector bias $V_p = +1$ V. The field is approximately uniform within the core of the device (shaded area). The trajectories of the electrons in the <111> valleys are drawn schematically (dashed arrowed lines) for an energy deposit at the center of the bottom surface of the crystal, in the hypothetical case that intervalley scattering could be neglected altogether. Electrons would then be collected by the *d* set of electrodes only.

Electron anisotropy in Ge at mK temperatures: experiment

2. EXPERIMENTAL SETUP

Experiments have been performed on two 200 gram coplanar grid detectors of the Edelweiss collaboration[5]. Device ID201 is *n*-type, ultra-pure germanium with N_d - N_a < 10^{10} cm^{-3}. Device ID203 is equally *n*-type with a net electrically active impurity concentration of 10^{11} cm^{-3}.[†] Both crystals are cut in the shape of a cylinder 48 mm in diameter and 20 mm thick, with its axis along the [001] orientation (fig.1). The orientation accuracy has been checked by X-ray diffraction, and found in both cases to be better than 2 degrees. The crystals are fitted on their flat surfaces with Al evaporated electrodes in the form of annular rings 200 nm thick and 0.2 mm wide with a 2 mm pitch. Guard electrodes on the outer area of the flat surfaces and on the lateral surface of the crystal complete the device.

Compared with the usual configuration of the Edelweiss detectors,[5] the electrode interconnections and the polarization scheme of these devices were modified to gain access to the effects of carrier straggling. To this end, the rings on the top surface of the crystal were connected together by ultrasonic bonding, giving five sets of collection electrodes of increasing radius from the face center, denoted by *a*, *b*, *c*, *d* and *g* respectively, and each fitted with a charge-sensitive amplifier. On the other hand, the electrodes on the bottom surface (including the lower guard) are all interconnected, forming the *h* measurement channel. The top surface electrodes are all set at the same bias potential V_p (denoted thereafter as the detector bias), and those on the bottom surface at the opposite potential -V_p relative to the detector casing at cryostat ground. This polarization scheme ensures that, except for two shallow areas (~ 1 mm thick) underneath the top and the bottom surfaces, the collection field is very nearly uniform in the core of the device, and parallel to the detector axis. Numerical resolution of the Laplace equation shows that the magnitude of the field is given approximately by $1.8V_p/D$ where D is the crystal thickness in cm, thus 0.9 V/cm for V_p = 1 V. A narrowly collimated ^{241}Am γ source is mounted alongside the detector axis, and generates 60 keV energy deposits within a small volume of a few mm^3 next to the center of the bottom surface. Comparative studies of electron and hole collection are thereby facilitated, as switching from one type of carrier to the other is simply done by inverting the bias polarities between the top and the bottom sets of electrodes. By respecting the cylindrical symmetry of the device, this setup also greatly simplifies the interpretation of the experimental data.

Measurements are made at 20 mK in a ^{3}He/^{4}He dilution refrigerator. Because of carrier trapping by defects and impurities, a gradual build-up of a space-charge takes place in the course of detector operation. A reproducible,

[†]The crystals were provided by Umicore (Olen, Belgium).

space-charge-free state of the Ge crystal is obtained prior to each set of measurements by an infra-red irradiation of the device using pulsed LED's.[6,7] For each value of the detector bias, a pattern of charge collection is recorded for the 60 keV energy deposits, consisting of the signal amplitudes in the six different measurement channels. These patterns characterize the amount of carrier straggle transverse to the detector axis, after the carriers were drifted from the site of energy deposition to the opposite side of the device.

3. CHARGE COLLECTION PATTERNS

Figures 2 and 3 present the charge collection patterns for electrons and holes respectively. The patterns are measured for detector biases between 0.5 and 12 V, which covers the full range of field intensities in the usual operating conditions of the Edelweiss detectors (typical collection fields in these devices are ~ 1 V/cm). Differences in electron and hole collection are apparent, as (except for the lower biases where a fraction of the holes spill out into the *b* measurement channel), holes collect in the *a* channel only, whose amplitude then identifies to that of the *h* channel. Electrons, on the other hand, exhibit more complex, bias dependent collection patterns which tend to resemble those for holes at the highest biases only.

As previously noted,[3] straggle effects in germanium at mK temperatures are thus much larger for electrons than for holes. As fig. 2 shows, the transverse straggle of the electrons at low detector biases ($V_p \leq$ a few V/cm) is on the macroscopic scale, and compares in magnitude to their projected path along the detector axis. By quantifying these effects, the collection patterns provide deeper insight into the nature of the scattering processes involved. Should carrier scattering be absent altogether, the electrons in all four energy valleys would propagate at an angle of ~ 35 degrees to the [001] detector axis, and would then be collected by the *d* set of electrodes only. That such is not the case brings into light, *a contrario,* the importance of the scattering processes (intervalley transitions via phonon emission in the first place[4,8]) in determining the form of the charge collection patterns. A comparison of the electron patterns in both devices shows furthermore that, in addition to lattice scattering, there is another process involved, effective at low collection fields and different by its effects from one device to the other. For the collection patterns, although identical at high detector biases ($V_p \geq$ ~ 8 V), become increasingly different at lower biases (with the amplitude *e.g.* in the *a* channel going through a maximum for $V_p = 4$ V in device ID203, while it just grows to a constant value below $V_p = 2$ V in device ID201). An explanation based on a difference in the crystallographic orientation of the

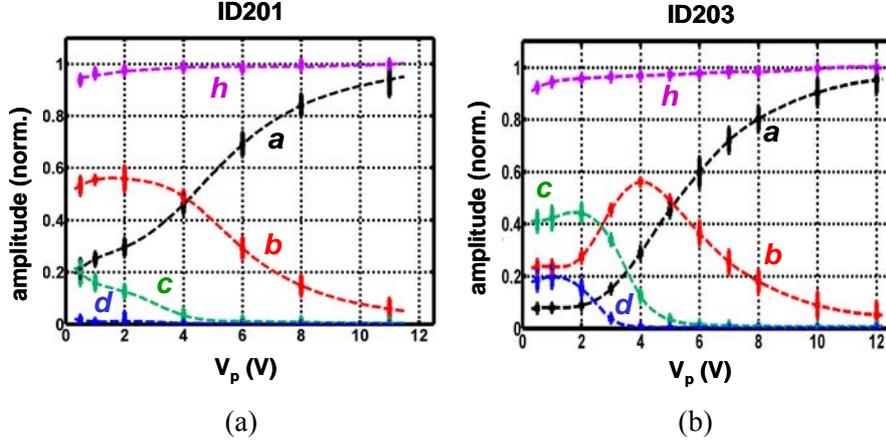**Electron anisotropy in Ge at mK temperatures: experiment**

ID201

ID203

Fig. 2. Electron collection patterns for the 60 keV energy deposits as a function of detector bias V_p (a) for device ID201 (*n*-type, ultra-pure Ge with $N_d - N_a < 10^{10}$ cm^{-3}) and (b) for device ID203 (*n*-type, $N_d - N_a = 10^{11}$ cm^{-3}), respectively. The signal amplitudes are normalized to unity for full charge collection in the *h* measurement channel. The dashed lines are guide for the eyes only. Data for each value of V_p correspond to ~ 400 recorded events. The standard deviation of the amplitudes about the mean is also represented. Data for channel *g* have been omitted, as this channel delivers zero signal amplitude for all bias voltages.
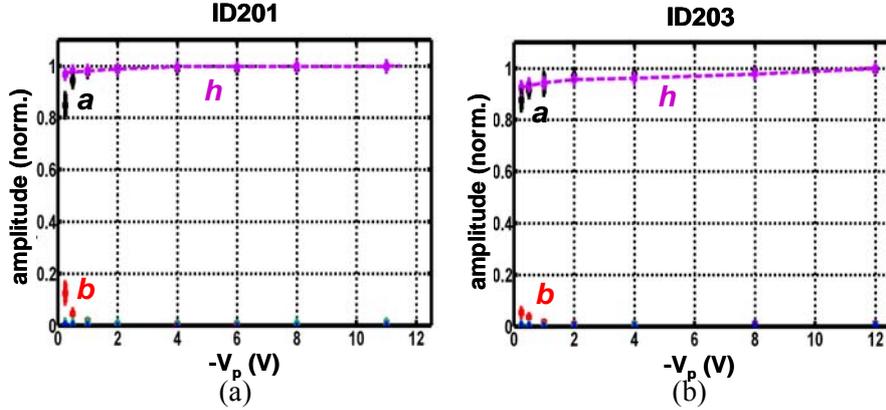
ID201

ID203

Fig. 3. Hole collection patterns for devices ID201 (a) and ID203 (b), respectively. Except for the lower detector biases ($|V_p| < ~ 1$ V), charge collection is between channels *a* and *h* only. Note enhanced hole trapping in device ID203 compared to ID201. This applies to electron trapping as well (fig. 2).

detector axes is excluded by our X-ray diffraction checks. On the other hand, the detector crystals differ by their impurity content, which strongly suggests an effect of impurity scattering, the more pronounced as the field is lower.[4] Another impurity-related effect is carrier trapping, as reflected in the *h* channel signal amplitudes. The latter channel measures the full collected charge, and thus registers the magnitude of the electron trapping effects, larger at low detector biases ($V_p < \sim 1V$) in the doped compared to the ultra-pure specimen (this applies to hole trapping as well).

4. SUMMARY

The results of this study summarize as follows:

(i) Electrons in cryogenic Ge detectors exhibit straggling effects on the macroscopic scale, with a transverse straggle comparable in magnitude to their projected path along the direction of the field.

(ii) The scattering processes involved differ depending on the field intensity. Lattice scattering predominates at fields larger than ~ 5 V/cm, whereas impurity scattering becomes increasingly important at lower fields.

(iii) The transverse straggle of holes is comparatively on a much smaller scale. The difference with electron straggle originates presumably from the streaming character of hot hole motion.[9]

(iv) The impurity effects vary in magnitude depending on the concentration of electrically active centers, which raises the question of the nature and the density of the impurities or defects involved.

A detailed analysis of the charge collection patterns in these devices is presented in a companion paper in these proceedings,[10] based on Monte Carlo simulations of carrier transport taking into account the combined effects on electron motion of intervalley and impurity scattering processes.

ACKNOWLEDGEMENT

REFERENCES

1. C. Jacoboni et al., *Phys. Rev. B* **24**, 1014 (1981).
2. L. Reggiani et al., *Phys. Rev. B* **16**, 2781 (1977).
3. B. Cabrera et al., e-print *arXiv*:1004.1233v1 [astro-ph.IM] (2010).
4. V. Aubry-Fortuna and P. Dollfus, *J. Appl. Phys.* **108**, 123706 (2010).
5. A. Broniatowski et al., *Phys. Lett. B* **681**, 305 (2009).

6. E. Olivieri et al., *Proc. 13th Int. Workshop on Low Temperature Detectors* (Stanford 2009, USA), *AIP Conf. Proc*. **1185**, 310 (2009).
7. J. Domange et al., *ibid.* 314.
8. K. M. Sundqvist and B. Sadoulet, *J. Low Temp. Phys.* **151**, 443 (2008).
9. W.E. Pinson and R. Bray, *Phys. Rev.* **136**, A1449 (1964).
10. A. Broniatowski, J. Low Temp. Phys. (2012) Proceedings LTD14. doi: 10.1007/s10909-012-0543-5.